AJNR

Epileptogenic Tubers Are Associated with Increased Kurtosis of Susceptibility Values: A Combined Quantitative Susceptibility Mapping and Stereoelectroencephalography Pilot Study

A. Chari, J. Sedlacik, K. Seunarine, R.J. Piper, P. Hales, K. Shmueli, K. Mankad, U. Löbel, C. Eltze, F. Moeller, R.C. Scott, M.M. Tisdall, J.H. Cross and D.W. Carmichael

Epileptogenic Tubers Are Associated with Increased Kurtosis of Susceptibility Values: A Combined Quantitative Susceptibility Mapping and Stereoelectroencephalography Pilot Study

A. Chari, J. Sedlacik, K. Seunarine, R.J. Piper, P. Hales, K. Shmueli, K. Mankad, U. Löbel, C. Eltze, F. Moeller, R.C. Scott, M.M. Tisdall, J.H. Cross, and D.W. Carmichael

ABSTRACT

BACKGROUND AND PURPOSE: Prior studies have found an association between calcification and the epileptogenicity of tubers in tuberous sclerosis complex. Quantitative susceptibility mapping is a novel tool sensitive to magnetic susceptibility alterations due to tissue calcification. We assessed the utility of quantitative susceptibility mapping in identifying putative epileptogenic tubers in tuberous sclerosis complex using stereoelectroencephalography data as ground truth.

MATERIALS AND METHODS: We studied patients with tuberous sclerosis complex undergoing stereoelectroencephalography at a single center who had multiecho gradient-echo sequences available. Quantitative susceptibility mapping and R2* values were extracted for all tubers on the basis of manually drawn 3D ROIs using T1- and T2-FLAIR sequences. Characteristics of quantitative susceptibility mapping and R2* distributions from implanted tubers were compared using binary logistic generalized estimating equation models designed to identify ictal (involved in seizure onset) and interictal (persistent interictal epileptiform activity) tubers. These models were then applied to the unimplanted tubers to identify potential ictal and interictal tubers that were not sampled by stereoelectroencephalography.

RESULTS: A total of 146 tubers were identified in 10 patients, 76 of which were sampled using stereoelectroencephalography. Increased kurtosis of the tuber quantitative susceptibility mapping values was associated with epileptogenicity ($P = .04$ for the ictal group and $P = .005$ for the interictal group) by the generalized estimating equation model. Both groups had poor sensitivity (35.0% and 44.1%, respectively) but high specificity (94.6% and 78.6%, respectively).

CONCLUSIONS: Our finding of increased kurtosis of quantitative susceptibility mapping values (heavy-tailed distribution) was highly specific, suggesting that it may be a useful biomarker to identify putative epileptogenic tubers in tuberous sclerosis complex. This finding motivates the investigation of underlying tuber mineralization and other properties driving kurtosis changes in quantitative susceptibility mapping values.

ABBREVIATIONS: DRE = drug-resistant epilepsy; GEE = generalized estimating equation; QSM = quantitative susceptibility mapping; SEEG = stereoelectroencephalography; TSC = tuberous sclerosis complex

Tuberous sclerosis complex (TSC) is a genetic disorder often associated with difficult-to-treat drug-resistant epilepsy (DRE).[1] While some studies report favorable outcomes following resective epilepsy surgery to treat TSC-associated DRE, others report that only about 50% become seizure-free following resective surgery, especially in complex cases with no clear dominant tuber.[2-6] There is an increasing practice of using stereoelectroencephalography (SEEG) to guide surgery in these patients, with a recognition that the best outcomes are achieved in patients with a clear "dominant" tuber and a focal putative seizure onset zone.[7]

However, targeting tubers as part of an SEEG implantation plan in these patients can be difficult because there is often a high tuber burden, semiology can be difficult to interpret, and video-electroencephalography lateralization and localization are often poor. The interpretation of neuroimaging is further complicated by heterogeneity in the appearance of tubers, with some imaging features more associated with epilepsy than others. One study identified 3 radiologically different tuber types based on T1-, T2-, and T2-FLAIR characteristics; the dominant type of tuber in a patient was associated with the likelihood of autism spectrum disorder, infantile spasms, and seizures, though no insights were drawn about the epileptogenicity of specific tubers.[8] Another study used this classification to quantitatively assess the epileptogenicity of tubers and the surrounding cortex during SEEG. It concluded that resection of the dominant tuber associated with a T2-FLAIR hypointense center, a higher epileptogenicity index compared with other tubers and the perituberal cortex, continuous interictal epileptiform discharges, and stimulation-induced seizures were associated with 80% seizure freedom. Outcomes were less favorable when there was a more complex organization of the epileptogenic zone.[9]

Studies have identified calcification as an indicator of DRE and epileptic foci in TSC, though these studies have predominantly used CT scans to assess whether there was calcification as a binary variable.[10,11] In the past few years, quantitative susceptibility mapping (QSM) has become more prevalent as a MR imaging technique, with the ability to detect intracranial calcification with high levels of sensitivity and specificity.[12] QSM is an advancement of SWI in which postprocessing techniques are applied to quantify the magnetic susceptibility of tissue. Its advantage is that it removes the blooming artifacts in SWI that are a factor of tissue geometry and orientation, leading to precise local quantification of magnetic susceptibility.[13] Magnetic susceptibility is increased by paramagnetic materials (hemorrhage, iron, gadolinium contrast) and decreased by diamagnetic materials (eg, calcification), and levels of these minerals have previously been shown to be altered in focal cortical dysplasia.[14] As part of the QSM processing, an R2* map is also generated, which is a measure of the amount of dephasing caused by B_0 field inhomogeneities either from macroscopic field perturbations or those due to local susceptibility effects.[13] In contrast to QSM, local field perturbations due to paramagnetic or diamagnetic materials have a similar effect.

In this exploratory pilot study, we sought to assess whether the QSM signal in tubers was able to identify putative epileptogenic tubers in a cohort of children with TSC undergoing SEEG as part of their presurgical evaluation for DRE. To explore the characteristics of the QSM distribution within each tuber, we assessed summary statistics of the histograms in each tuber (median, upper quartile, lower quartile, skewness, and kurtosis). We hypothesized that QSM and the associated R2* values would differ between epileptogenic and nonepileptogenic tubers, with epileptogenic tubers having lower QSM and higher R2* values as a result of increased calcium content and that this difference may affect both the median values and skewness of the distributions.

MATERIALS AND METHODS
This was a single-center retrospective cohort study reported according to the STrengthening the Reporting of OBservational studies in Epidemiology (STROBE) guidelines. Because it used routinely collected clinical data, ethics approval and the need for individual patient informed consent was waived by the research and development department at Great Ormond Street Hospital, and this study was registered as a clinical audit with the clinical audit department at Great Ormond Street Hospital.

We studied a series of consecutive patients with TSC undergoing SEEG evaluation between January 2016 and December 2020 and who also had multiecho gradient-echo imaging suitable for QSM as part of their routine clinical MR imaging before SEEG was available for study inclusion. The decision to perform SEEG, the interpretation of the SEEG results, and offers of resective surgery were collected by the epilepsy surgery multidisciplinary team without reference to the QSM data.

Image Acquisition
Images were acquired using a 3T MR imaging scanner (Magnetom Prisma; Siemens) with a 20-channel head and neck receive coil. The image-acquisition parameters for the anatomic T1-weighted 3D-MPRAGE scan were the following: TI = 900 ms, TR = 2300 ms, TE = 2.74 ms, flip angle = 8°, readout bandwidth = 200 Hz/pixel, 1-mm^3 isotropic voxel size, acquisition matrix = 256 × 256 × 240, parallel acquisition acceleration factor = 2, coronal orientation, total scan time = 5 minutes 19 seconds.

The image acquisition parameters for the 3D T2-FLAIR were the following: TI = 1800 ms, TR = 5000 ms, TE = 395 ms, echo-train length = 233 with variable flip angle optimized for T2-weighting, readout bandwidth = 650 Hz/pixel, acquisition matrix = 384 × 291 × 240 reconstructed to 0.65 × 0.65 × 1 mm^3 voxel size, parallel acquisition acceleration factor = 2, coronal orientation, total scan time = 6 minutes 10 seconds.

The image acquisition parameters for the R2*/QSM 3D multiecho gradient-echo sequence were the following: TEs = 3, 7, 11, 15, 19, 23, and 27 ms, TR = 38 ms, flip angle =15°, readout bandwidth = 360 Hz/pixel, acquisition matrix = 192 × 156 × 144 reconstructed to 0.6-mm^3 isotropic voxel size, 6/8 partial Fourier factor in phase- and section-encoding directions, parallel acquisition acceleration factor = 2 in a phase-encoding direction, transverse orientation, total scan time = 5 minutes 41 seconds.

QSM Processing
Single-channel image data were combined for each TE by the sum of squares of all single-channel magnitude images. The combined phase image φ was calculated for each TE by the sum of conjugate complex multiplication between the previous and current TEs. The conjugate complex multiplication eliminates the incongruous spatial phase sensitivies of each coil element, allowing the phase correct summation of the complex image data. The combined phase image of the first TE was set to zero.

$$\phi_{TE_1} = 0$$
$$\phi_{TE_n} = arg\left(\sum z_{TE_{n-1}} \cdot \bar{z}_{TE_n}\right) \forall n > 1 .$$

A brain mask was computed on the first echo magnitude image using the FSL Brain Extraction Tool (http://fsl.fmrib.ox.ac.uk/fsl/fslwiki/BET).[15] The R2* map was calculated on the logarithmic

magnitude images using the Moore-Penrose pseudoinverse implementation. The frequency shift was calculated from the combined phase images of all TEs using the Fit_ppm_complex.m function in the MEDI toolbox (https://github.com/huawu02/MEDI_toolbox/blob/main/UPDATES.m).[16] The local frequency shift was calculated using the projection onto dipole fields method with an eroded brain mask (85% of the original size of the FSL BET brain mask) to minimize nonlocal phase contributions.[17] The QSM map was then calculated from the local frequency shift using the iterative Tikhonov dipole inversion method.[18]

Image Processing

Manual segmentation of all visible tubers was performed using coregistered volumetric T1- and T2-FLAIR MR imaging using ITK-SNAP (www.itksnap.org).[19] This was performed by the first author (A.C.), who is a neurosurgical resident with experience in pediatric epilepsy, under the supervision of a neuroradiologist with a special interest in pediatric epilepsy (K.M.). To reduce QSM artifacts from the pial surface vessels, we limited the manual segmentations to 1–2 mm away from the pial surface (Fig 1A). Manual visual checks were performed to ensure that all implanted tubers were segmented.

Imaging from the SEEG (including the electrode locations), the QSM and R2* maps, and postoperative scans were coregistered to the original volumetric T1 and validated visually (Fig 1A). Using these coregistered maps and the report from the SEEG procedure, we classified each segmented tuber as being implanted or not and, if implanted, whether it was labeled as having ictal epileptiform activity (ie, part of the seizure onset zone, "ictal") or interictal epileptiform activity ("interictal"). This classification was based on the SEEG report, which was completed by the clinical team including a consultant neurophysiologist, consultant neurologist, and consultant neurosurgeon with experience in SEEG. The definition of "ictal" was that there was electrophysiologic change in the tuber at seizure onset, and the tuber was identified as one that should be resected as part of any surgery were it to be offered. The definition of "interictal" was persistent interictal epileptiform discharges in the tuber. In addition, note was made of whether the tuber was resected from the postoperative imaging.

Statistical Analysis

QSM and R2* values from each tuber were extracted on the basis of the coregistered QSM and R2* maps. To characterize the distribution of quantitative data from each tuber, we extracted the size of the tuber (number of voxels) and the median, upper quartile, lower quartile, skewness, and kurtosis of the QSM and R2* maps for each tuber (Fig 1B).

Using the values above (11 variables in total), 2 generalized estimating equation (GEE) binary logistic regression models were constructed using only the implanted tubers to assess whether there were factors that were predictive of whether the tuber was ictal or interictal. GEE models accommodate for repeated measures, which, in this case, are the potential intrasubject correlation between many tubers in the same patient. Following evaluation of model specificity and sensitivity, these model parameters were then applied to the unimplanted tubers to predict ictal and interictal tubers from the unimplanted tubers and assess whether the predicted unresected ictal and interictal tuber burden correlated with the outcome following SEEG-guided resective epilepsy surgery.

Software, Data, and Code Availability Statement

All image processing was performed using the tools described above and in-house scripts in Matlab, Release 2020b (MathWorks) for QSM processing and data extraction and SPSS (IBM) for GEE modeling. Code is available at www.github.com/aswinchari/QSM. The GitHub repository contains the tuber information used to construct the GEE models. Coregistered imaging data are available from the corresponding authors on reasonable request.

RESULTS

Clinical Results

During the 5-year period, 14 children with TSC underwent SEEG. One child had previously undergone tuber resection, while another had undergone resective surgery for a subependymal giant cell astrocytoma. In 12 children (85.7%), a seizure-onset zone was identified following SEEG, and resective surgery was offered. All except 1 child had undergone resective surgery, including resection of single tuber and multiple tubers ± mesial temporal structures.

At a median follow-up of 2.0 years (range, 1.0–4.3 years), 2 patients (18.2%) had an Engel Class I outcome, 3 (27.3%) had an Engel Class II outcome, 5 (45.4%) had an Engel Class III outcome, and 1 (9.1%) had an Engel Class IV outcome.

QSM and R2* Results

Of the 14 patients, 11 had undergone QSM as part of their preoperative scans, but 1 patient had to be excluded due to artifacts from dental braces. Therefore, the scans of 10 patients were included in the subsequent analyses (Online Supplemental Data). From these patients, a total of 146 tubers were masked (range, 6–23 tubers per patient), of which 76 were sampled by SEEG electrodes (range, 4–13 tubers per patient) and 70 were not. Of the sampled tubers, 20 were labeled as ictal, and 34, as interictal.

By means of the 76 tubers sampled by SEEG electrodes, 2 binary logistic GEE models were constructed to predict whether tubers were involved in ictal onset (ictal model) or interictal activity (interictal model). For both models, the only factor independently associated with ictal or interictal status was the kurtosis of the QSM histogram ($P = .04$ for the ictal model and $P = .005$ for the interictal model) (Online Supplemental Data). The predictions of the models were used to assess whether they correctly categorized the implanted tubers; both models had poor sensitivity (35.0% and 44.1%, respectively) but high specificity (94.6% and 78.6%, respectively) (Fig 2A).

The developed model parameters were subsequently applied to the test data set of unimplanted tubers. They identified 10 tubers as ictal and 27 as interictal, of which 7 were overlapping. These were spread across most of the subjects with a range of 0–4 additional ictal tubers and 0–6 additional interictal tubers identified that were not sampled by SEEG (Online Supplemental Data).
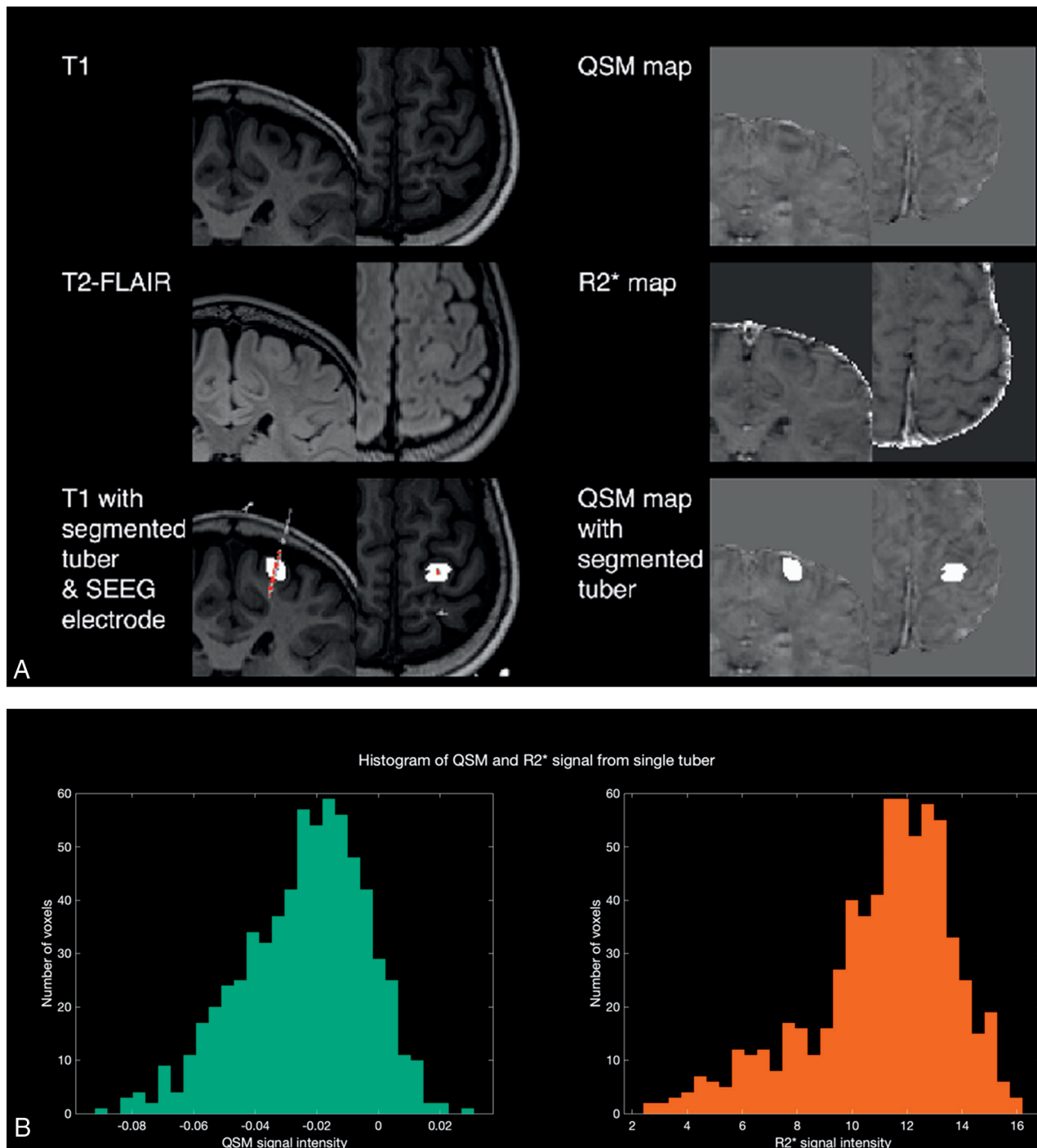
FIG 1. Methods summary. *A*, Illustrative images of T1-, T2-FLAIR, segmented tubers and overlying electrodes, QSM, and R2* maps used in this study. *B*, Histograms show distributions of QSM and R2* values for the left motor strip tuber identified in *A*.

Figure 2*B* shows the distribution of QSM kurtosis values across all tubers that were implanted and from the model predictions. This shows the association between higher kurtosis (heavier tails of QSM values) and ictal and interictal tubers. Similar trends were not seen when plotting the median QSM values across all tubers (Fig 2*C*).

Last, the predictions of the models were used to assess whether there was a linear association between the Engel outcome and the total number of unresected predicted ictal and interictal tubers (Fig 3). Although there was a modest positive relationship for the ictal model, the regression coefficients were not statistically significant for either model (ictal regression coefficient = 0.42, R^2 = 0.23, P = .16; interictal regression coefficient = 0.10, R^2 = 0.003, P = .88).

Illustrative Example
As an example, we present the case of a 10-year-old child diagnosed with TSC at 11 months of age with 4 different seizure types,
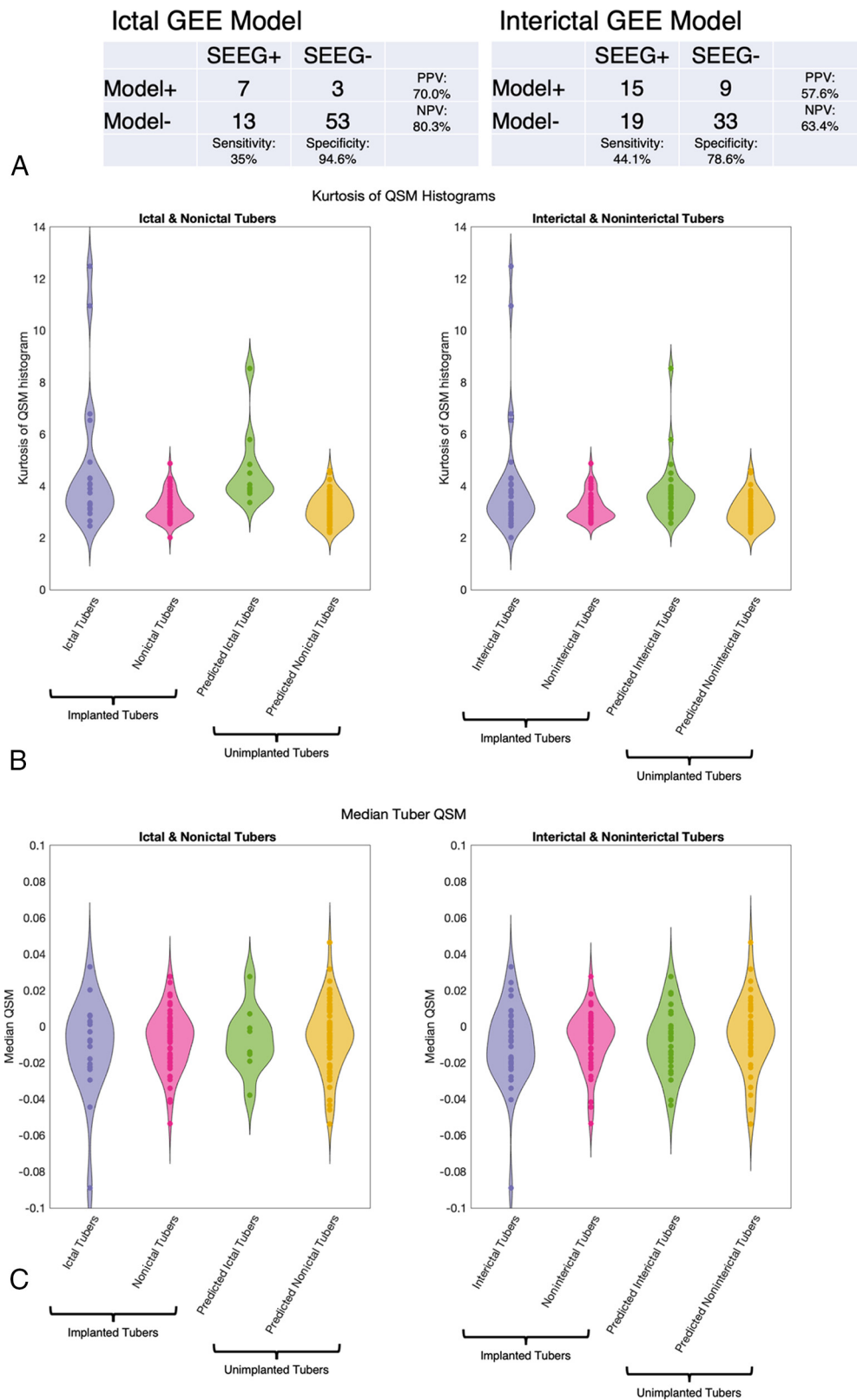
FIG 2. Output of GEE models. *A,* The 2 × 2 tables illustrate the sensitivity and specificity of the developed models to identify ictal and interictal tubers in the implanted tubers *B,* Violin plots of the kurtosis of the QSM histograms across implanted and nonimplanted tubers show higher kurtosis in the SEEG-identified and model-predicted ictal and interictal tubers, albeit with a degree of overlap. *C,* Violin plots of the median QSM values across implanted and nonimplanted tubers show higher kurtosis in the SEEG-identified and model-predicted ictal and interictal tubers, showing no difference between groups.

Association Between Outcome and Predicted Ictal/Interictal Unresected Tubers

FIG 3. Association between model-predicted unresected tubers and postoperative Engel outcomes. There was no significant correlation between outcome and the total number of unresected ictal and interictal tubers predicted by the model (ictal regression coefficient = 0.42, R2 = 0.23, P = .16; inter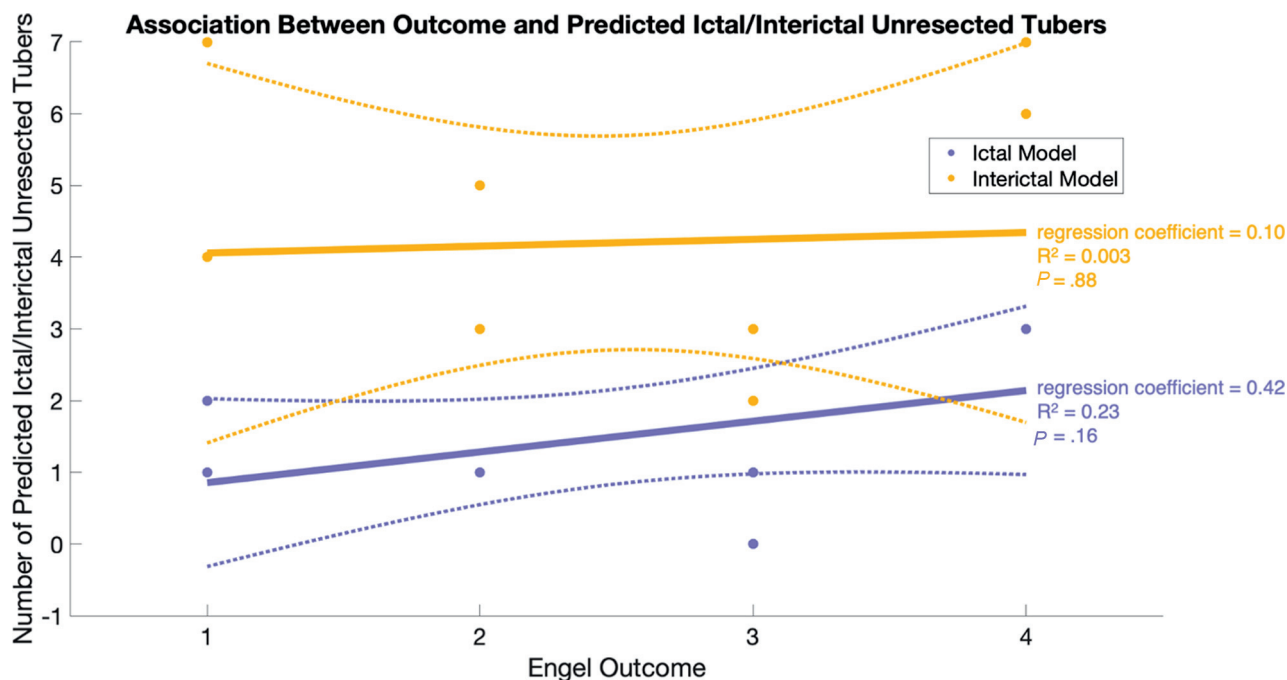ictal regression coefficient = 0.10, R2 = 0.003, P = .88). Note that for this analysis, 2 patients who did not undergo subsequent surgical intervention were classified as Engel class IV, and the Engel class was considered a linear variable.

including, most commonly, asymmetric spasms with more right-body involvement than left. Ictal video telemetry recordings for 3 seizure types lateralized to the left hemisphere, while one lateralized to the right. Interictal EEG showed bilateral epileptiform activity, but this was more pronounced on the left. MR imaging showed evidence of bilateral tubers with no clear dominant tuber. An interictal magnetoencephalogram was performed, showing interictal activity in the left prefrontal and temporoparietal regions. On the basis of the findings above, a bilateral SEEG implantation was planned with more left-sided than right-sided sided electrodes (Fig 4A). This identified 2 tubers involved in seizure onset (Fig 4B, red tubers). These tubers were subsequently resected, and 2 years after the operation, the patients had an Engel Class III outcome with significant reduction in seizure frequency and duration and associated improvement in cognition and attention.

The ictal GEE model using the QSM data identified an additional potential epileptogenic tuber in the right occipital region (Fig 4B, green tuber), which was not sampled by the SEEG electrodes. The normalized QSM histograms of all 3 tubers are shown, illustrating a narrower width and, therefore, increased kurtosis compared with all the other 15 tubers in the same patient (Fig 4C).

DISCUSSION

To our knowledge, this is only the second study to use QSM in TSC and the first to quantitatively analyze the QSM characteristics. The previous study showed that QSM was feasible in the context of identifying calcifications in both tubers and subependymal nodules.

On the basis of the ground truth of SEEG interpretation, we found that a model containing QSM and R2* signal characteristics may be helpful in identifying putative epileptogenic tubers in TSC with a high level of specificity but low sensitivity (Fig 2A). This finding suggests that preoperative QSM may be a useful adjunct for the selection of tubers for SEEG exploration because ictal lesions nearly always had high kurtosis in our sample. These results warrant prospective assessment. Specifically, epilepsy in TSC can be associated with complex networks; therefore, tubers distant from the regions identified by semiology and video-electroencephalography may be involved in seizure generation and warrant sampling.[7] Most interesting, most patients in this cohort (8/10) had additional unimplanted tubers identified as potentially epileptogenic by the model, which, combined with the evidence that only 2 patients had an Engel Class I outcome, provides preliminary evidence that these additional tubers may have been worthwhile to sample as part of the SEEG exploration. The poor correlation of unresected predicted ictal tubers with outcome (Fig 3) is explained by the poor sensitivity of the model, and further prospective work might identify additional features to improve the sensitivity, such as other modalities of MR imaging incorporated into the model or data such as electrical source modeling.[20] However, the high specificity suggests that the models may be useful in the prospective identification of putative epileptogenic tubers that could then be targeted for confirmation through SEEG recordings. Indeed, there is a precedent for using radiologic biomarkers to identify additional areas to explore during SEEG.[21]

In our GEE models, we identified the kurtosis of the QSM signal histogram being significantly associated with both ictal
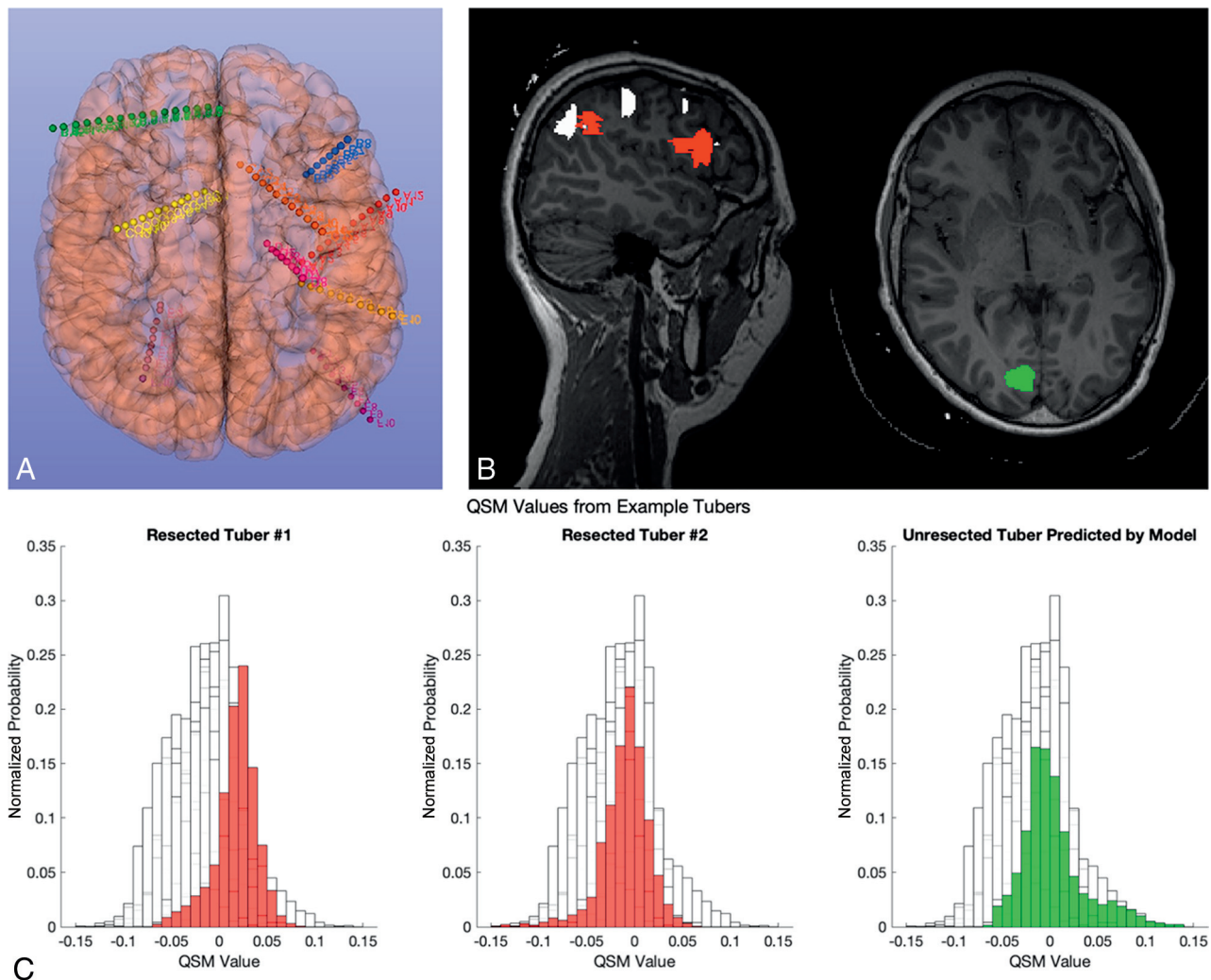
FIG 4. Illustrative case example. *A*, Illustration of bilateral SEEG implantation with a more left-sided electrode. *B*, Sagittal and axial T1 images with overlying tuber segmentation. The 2 identified epileptogenic tubers that were subsequently resected are shown in red, while a third tuber in green was not sampled but identified as potentially epileptogenic by the GEE model. *C*, Histograms of the QSM values of the 3 tubers shown in *B* overlaid on the histograms of 15 other tubers from the same patient (in white). Note that they all seem to have a higher kurtosis.

($P = .04$) and interictal ($P = .005$) tubers, with increased kurtosis in epileptogenic tubers without significant changes in the median QSM values. This finding suggests that although there may not necessarily be an average increase in the calcium content within epileptogenic tubers, the distribution of QSM values had thicker tails. Increased kurtosis of QSM values being associated with epileptogenicity is a novel finding and requires both a biologic explanation and external validation, especially because it does not fully agree with previous studies that indicate calcification as a marker of epileptogenicity.[10,11] For example, Lorio et al[14] found decreased QSM values, corresponding to increased calcium and zinc in focal epileptogenic lesions such as in focal cortical dysplasia type IIb. The high kurtosis in this study could be explained by the thicker tails on both sides of the distribution, indicating areas of low susceptibility (eg, from high calcium) and high susceptibility (eg, from areas of increased blood flow or iron deposition) compared with nonepileptogenic tubers.

Indeed, alterations of iron deposition have also been described in radiologically classified tubers of focal cortical dysplasia; these

require electrophysiologic and histopathologic correlation, which may give insight into why certain radiologic characteristics (for example, high QSM kurtosis or low T2-FLAIR intensity) are associated with epileptogenicity. This knowledge may aid the targeting of putative epileptogenic tubers in future SEEG implantations. In addition, our model does not account for the dynamics of epileptogenicity within a tuber, where the core, periphery, and perituberal tissue may contribute differently to seizure onset; again, this issue would require further study.[9] QSM signal distributions have also been linked to a chronic inflammatory response and glial activation in MS lesions,[22] and it would, therefore, be interesting to correlate longitudinal imaging findings with markers of epileptogenicity and, ultimately, histology to understand the potential role of inflammation in tubers and how they contribute to epileptogenesis.

The study has a number of limitations. First, it is a small single-center retrospective series that requires internal prospective and external validation. The cohort was small, and only 18% of subjects were seizure-free at last follow-up, indicating a complex

cohort. QSM is also inherently associated with artifacts, such as from the cortical surface, which may have affected the results; despite our attempts to reduce such artifacts, novel postprocessing pipelines may help reduce them further.[23] The utility of the model would also be improved by understanding the biologic basis for increased kurtosis leading to epileptogenicity, such as postoperative analysis of tissue mineral content. The tubers were segmented using only the T1- and T2-FLAIR sequences. It is conceivable that incorporating the QSM maps into the interpretation of tuber characteristics may aid radiologic interpretation of the nature and extent of tubers.

We were unable to include quantitative analyses of T1- and T2-FLAIR signal characteristics, CT scan densities, and the SEEG signals in this study, but these may be useful constructs for future studies for quantitatively assessing associations between CT/MR imaging signal characteristics and quantitative markers of SEEG epileptogenicity. Existing SEEG markers of epileptogenicity include cortico-cortical evoked potentials, neuronal spiking activity and fast ripples, and more in-depth analyses could relate QSM characteristics to these.[24-26] In addition, there may be a more nuanced interpretation of SEEG in TSC that we have not considered; the ethos at our institution is to consider tubers as individual entities being either involved or not involved in the seizure onset, but we acknowledge that other schools may consider parts of tubers or perituberal tissue to be epileptogenic; therefore, future studies may seek to assess QSM signal characteristic distributions within and around tubers as markers of epileptogenic tissue. There is also a possibility of dynamic changes in QSM signals, which were not captured in this study because the postoperative imaging protocols did not include QSM in our institution.

CONCLUSIONS

Despite these limitations, this study provides important proof of principle that quantification and assessment of tuber mineral content through QSM may be a useful biomarker in the identification of the putative epileptogenic tubers in TSC. Most important, our results, that high kurtosis is associated with epileptogenicity with a high specificity and low sensitivity, did not support our hypothesis that epileptogenicity would be associated with increased calcium and, therefore, a greater prevalence of lower QSM values. This result does not refute the hypothesis that calcification is an important marker in tuber epileptogenicity but may indicate a more complex process. Increased QSM kurtosis could involve changes in mineral content (eg, calcium and iron) and perhaps inflammation and blood flow changes, all of which may relate to epileptogenicity. Larger cohorts, external validation, and correlation with histologic and tissue mineral analysis are required to further this work.

Disclosure forms provided by the authors are available with the full text and PDF of this article at www.ajnr.org.

REFERENCES

1. Nabbout R, Belousova E, Benedik MP, et al. **Historical patterns of diagnosis, treatments, and outcome of epilepsy associated with tuberous sclerosis complex: results from TOSCA Registry.** *Front Neurol* 2021;12:697467 CrossRef Medline

2. Arya R, Tenney JR, Horn PS, et al. **Long-term outcomes of resective epilepsy surgery after invasive presurgical evaluation in children with tuberous sclerosis complex and bilateral multiple lesions.** *J Neurosurg Pediatr* 2015;15:26–33 CrossRef Medline

3. Fallah A, Guyatt GH, Snead OC, et al. **Predictors of seizure outcomes in children with tuberous sclerosis complex and intractable epilepsy undergoing resective epilepsy surgery: an individual participant data meta-analysis.** *PLoS One* 2013;8:e53565 CrossRef Medline

4. Fallah A, Rodgers SD, Weil AG, et al. **Resective epilepsy surgery for tuberous sclerosis in children: determining predictors of seizure outcomes in a multicenter retrospective cohort study.** *Neurosurgery* 2015;77:517–24; discussion 524 CrossRef Medline

5. Liu S, Yu T, Guan Y, et al. **Resective epilepsy surgery in tuberous sclerosis complex: a nationwide multicentre retrospective study from China.** *Brain* 2020;143:570–81 CrossRef Medline

6. Specchio N, Pepi C, de Palma L, et al. **Surgery for drug-resistant tuberous sclerosis complex-associated epilepsy: who, when, and what.** *Epileptic Disord* 2021;23:53–73 CrossRef Medline

7. Park JT, Vaca GF. **Stereo-EEG in tuberous sclerosis complex.** *Pediatr Neurol Briefs* 2020;34:6 CrossRef Medline

8. Gallagher A, Grant EP, Madan N, et al. **MRI findings reveal three different types of tubers in patients with tuberous sclerosis complex.** *J Neurol* 2010;257:1373–81 CrossRef Medline

9. Neal A, Ostrowsky-Coste K, Jung J, et al. **Epileptogenicity in tuberous sclerosis complex: a stereoelectroencephalographic study.** *Epilepsia* 2020;61:81–95 CrossRef Medline

10. Altman NR, Purser RK, Post MJ. **Tuberous sclerosis: characteristics at CT and MR imaging.** *Radiology* 1988;167:527–32 CrossRef Medline

11. Zhang MN, Zou LP, Wang YY, et al. **Calcification in cerebral parenchyma affects pharmacoresistant epilepsy in tuberous sclerosis.** *Seizure* 2018;60:86–90 CrossRef Medline

12. Chen W, Zhu W, Kovanlikaya I, et al. **Intracranial calcifications and hemorrhages: characterization with quantitative susceptibility mapping.** *Radiology* 2014;270:496–505 CrossRef Medline

13. Ruetten PP, Gillard JH, Graves MJ. **Introduction to quantitative susceptibility mapping and susceptibility weighted imaging.** *Br J Radiol* 2019;92:20181016 CrossRef Medline

14. Lorio S, Sedlacik J, So PW, et al. **Quantitative MRI susceptibility mapping reveals cortical signatures of changes in iron, calcium and zinc in malformations of cortical development in children with drug-resistant epilepsy.** *Neuroimage* 2021;238:118102 CrossRef Medline

15. Jenkinson M. **BET: MR-Based Estimation of Brain, Skull and Scalp Surfaces.** In: *Proceedings of the Annual Meeting of the Organization for Human Brain Mapping*, Toronto, Ontario, Canada. June 12–16, 2005

16. Liu T, Wisnieff C, Lou M, et al. **Nonlinear formulation of the magnetic field to source relationship for robust quantitative susceptibility mapping.** *Magn Reson Med* 2013;69:467–76 CrossRef Medline

17. Liu T, Khalidov I, de Rochefort L, et al. **A novel background field removal method for MRI using projection onto dipole fields (PDF).** *NMR Biomed* 2011;24:1129–36 CrossRef Medline

18. Karsa A, Punwani S, Shmueli K. **An optimized and highly repeatable MRI acquisition and processing pipeline for quantitative susceptibility mapping in the head-and-neck region.** *Magn Reson Med* 2020;84:3206–22 CrossRef Medline

19. Yushkevich PA, Piven J, Hazlett HC, et al. **User-guided 3D active contour segmentation of anatomical structures: significantly improved efficiency and reliability.** *Neuroimage* 2006;31:1116–28 CrossRef Medline

20. Centeno M, Tierney TM, Perani S, et al. **Combined electroencephalography-functional magnetic resonance imaging and electrical source imaging improves localization of pediatric focal epilepsy.** *Ann Neurol* 2017;82:278–87 CrossRef Medline

21. Chari A, Adler S, Wagstyl K, et al. **IDEAL approach to the evaluation of machine learning technology in epilepsy surgery: protocol for the MAST trial.** *BMJ Surg Interv Health Technol* 2022;4:e000109 CrossRef Medline

22. Gillen KM, Mubarak M, Park C, et al. **QSM is an imaging biomarker for chronic glial activation in multiple sclerosis lesions.** *Ann Clin Transl Neurol* 2021;8:877–86 CrossRef Medline

23. Yaghmaie N, Syeda WT, Wu C, et al. **QSMART: quantitative susceptibility mapping artifact reduction technique.** *Neuroimage* 2021;231:117701 CrossRef Medline

24. Wang Y, Yuan L, Zhang S, et al. **Fast ripples as a biomarker of epileptogenic tuber in tuberous sclerosis complex patients using stereo-electroencephalograph.** *Front Hum Neurosci* 2021;15:680295 CrossRef Medline

25. Yu X, Ding P, Yuan L, et al. **Cortico-cortical evoked potentials in children with tuberous sclerosis complex using stereo-electroencephalography.** *Front Neurol* 2019;10:1093 CrossRef Medline

26. Despouy E, Curot J, Denuelle M, et al. **Neuronal spiking activity highlights a gradient of epileptogenicity in human tuberous sclerosis lesions.** *Clin Neurophysiol* 2019;130:537–47 CrossRef Medline